Evidence of Highly Localized Failure within Core−Shell Toughening Particles from in-Situ Small-Angle Scattering

Michele Sferrazza,[†,‡] Jane Crawshaw,[†] Athene M. Donald,*[,†] and Theyencheri Narayanan[§]

Cavendish Laboratory, University of Cambridge, Madingley Road, Cambridge CB3 0HE, U.K.; Department of Physics, School of Physics and Chemistry, University of Surrey, Guildford, GU2 7XH; and ESRF, BP 220, F-38043 Grenoble Cedex, France

Received December 4, 2000; Revised Manuscript Received July 9, 2001

ABSTRACT: In-situ tensile deformation of toughened PMMA was investigated using small-angle X-ray scattering (SAXS). The toughening particles had a three-layer structure consisting of a PMMA core, a rubber shell, and a thin PMMA outer layer. Uniaxial tensile stress was applied at a constant strain rate of 5 mm/min at room temperature. Under these conditions the dominant deformation mechanism was found to depend on the concentration of toughening particles. When the particle concentration was low, the SAXS patterns showed that highly localized failure occurred inside the particles as the yield point of the tensile curve was reached. The failure began at the poles of the particles, at or immediately adjacent to the core/shell interface, and during yield it grew around this interface. At high particle concentration the particles stretched without failing. No evidence for crazing was seen in any of the scattering patterns. The major deformation mechanisms occurred inside the toughening particles rather than in the PMMA matrix.

Introduction

The subject of rubber toughening has reemerged in recent years as an issue of scientific controversy, with the realization that crazing is not necessarily the only toughening mechanism operating in many toughened polymer matrices[1−3] and indeed may not be a source of toughness at all.[4] This was first demonstrated in a small-angle X-ray scattering (SAXS) study on high-impact polystyrene (HIPS), under tensile strain, which showed that crazing only contributed to half the total plastic strain and that noncrazing mechanisms occurred before crazing.[1] This initial work of Kramer et al.,[1] using HIPS under impact conditions, indicated how real time investigations using a synchrotron source, coupled with so-called invariant analysis, permit a quantitative determination of the extents of crazing and noncrazing processes operating at different stages of deformation. When crazes are the only scattering centers in a polymer system, the overall shape of the SAXS pattern is a cross[1,5,6] formed by scattering perpendicular to the tensile axis (equatorial scattering) produced by the craze fibrils and scattering parallel to the tensile axis (meridional scattering) produced by the craze−bulk interfaces. However, in more recent work by Magalhaes et al.,[4] on a similar system of toughened polystyrene, a significant amount of scattering was observed at much lower angles than the peak originating from the craze fibril scattering. This lower angle scattering must originate from an alternative mechanism to crazing. One example of a noncrazing mechanism is rubber particle cavitation, which has been modeled using an energy balance approach by Lazzeri and Bucknall[2] and Bucknall, Karpodinis, and Zhang.[3] Other workers have begun to find evidence for the role of noncrazing mechanisms in toughened polymers where crazing was traditionally thought to dominate.[7−9] The original crazing model for toughening, in which the rubber particles only acted as sites for initiating a large number of crazes, is therefore no longer thought to be adequate.

It follows that in a rubber toughened polymer crazing is not the only possible deformation mechanism which can produce scattering in the small-angle region. Furthermore, depending on the particle size and morphology, scattering from the particles themselves may contribute to accessible regions of the scattering pattern. Therefore, it is important to be able to distinguish the different possible contributions to the scattering pattern. For the work described in this paper and in previously published[10−12] work by the group, the rubber-modified system investigated was PMMA toughened with three-layer core−shell type particles, consisting of a PMMA core, rubber middle layer, and thin PMMA outer layer. Initial real time SAXS studies[10,11] on in-situ deformation of this rubber toughened PMMA (RTPMMA) system showed that the contribution of the particle form factor scattering must be taken into account when analyzing SAXS patterns. The form factor scattering shows that the particle deformation is inhomogeneous, meaning that the rubber shell deforms more than the glassy core. This work was continued with an investigation of the effect on deformation mechanisms of both the rubber particle concentration and cross-linking density of the rubber.[12] In certain RTPMMA specimens, late stages of deformation have been accompanied by a four-point scattering pattern at very low scattering angle, and this has been interpreted as the possible signature of aligned cavitated particles in dilation bands, after the work of Lazzeri and Bucknall.[2]

This earlier work was done at a strain rate of 0.5 mm/min. This paper reports a real time SAXS study of tensile deformation of RTPMMA at the higher strain rate of 5 mm/min, designed to look in the very low-q region of the scattering pattern to explore deformation within the core−shell toughening particles.

[†] University of Cambridge.
[‡] University of Surrey.
[§] ESRF.

10.1021/ma002060v CCC: $20.00
Published on Web 08/16/2001

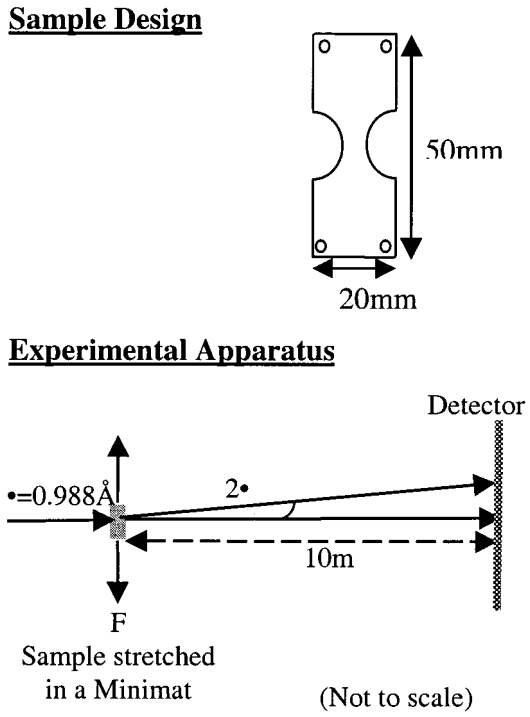

Figure 1. Sample design and schematic of arrangement of simultaneous SAXS and tensile test apparatus.

Experimental Section

Rubber toughened poly(methyl methacrylate) (RTPMMA) was investigated for the work described here. The toughening particles have a three-layer structure consisting of a PMMA core of radius 800−850 Å, a cross-linked rubber middle layer 400−500 Å thick, and a thin PMMA outer layer approximately 100 Å thick. The rubber middle layer was composed of poly[(*n*-butyl acrylate)-*co*-styrene] with a 4:1 weight ratio of *n*-butyl acrylate to styrene, and the outer PMMA layer is present to ensure good adhesion between the particle and the PMMA matrix. These toughening particles were a model system provided by ICI Acrylics plc (now INEOS Acrylics), where they were prepared by sequential emulsion polymerization. The cross-linking density of the rubber layer was controlled by the level of allyl methacrylate, and samples used here had 1%, 2%, and 5% cross-linking density, quoted by weight of the rubber layer.

Samples with toughening particle concentrations ranging from 10 to 40 wt % were prepared. For in situ tensile testing, RTPMMA specimens had overall dimensions of 32 mm × 20 mm and thickness 1.2−1.5 mm. A stress concentration region was created in the sample, in the form of a pair of semicircular cuts, to ensure that deformation occurred in the path of the X-ray beam. Care was taken to ensure that there was no damage to the samples during machining to produce the stress concentrators. The sample design is shown in Figure 1 together with the arrangement of the apparatus for simultaneous SAXS and tensile test.

The nonuniform sample shape means that value of precise local strains and stresses are hard to obtain, although load−extension curves could be recorded simultaneously with the scattering patterns. The specimens were mounted in a Polymer Laboratories Minimat tensometer, with the tensile axis vertical and the beam incident at the center of the specimen. The extension rate was 5 mm/min, and the experiments were carried out at room temperature (i.e., 20 °C).

The SAXS experiments were performed at the ID2 beamline of the European Synchrotron Radiation Facility (ESRF), Grenoble (France). The incident monochromatic radiation of wavelength 0.988 Å combined with a camera length of 10 m, allowed access to a much lower scattering vector (q) range than can usually be obtained. [The positions in the scattering pattern will be described in terms of the magnitude of the scattering vector, $\mathbf{q}$, where $|\mathbf{q}| = 4\pi \sin(\theta)/\lambda$, where 2θ is the scattering angle and λ is the X-ray wavelength.] The q range available was 0.0025−0.05 Å^{-1}, permitting investigation of Bragg spacings ($d \cong 2\pi/q$) up to 2500 Å. The X-ray beam had a cross section at the sample of approximately 0.3 mm × 0.9 mm and a typical flux of 8×10^{12} photons/s at 12 keV. The ID2 beam line is equipped with an image intensifier CCD system consisting of 1024 × 1024 pixels (pixel size ∼ 178 × 178 μm^2). The q range in both vertical and horizontal directions was calibrated using a grid having a hole separation of 0.5 cm and measuring the scattering of a water sample in the specimen position. The incident beam flux was monitored by a silicon PIN diode, which measures the scattering from a thin Kapton foil. A small silicon PIN diode embedded in the beam-stop directly measures the transmitted beam flux. Background scattering was subtracted from the data. Correction was made for spatial distortion and the detector efficiency. The standard procedure for SAXS data treatment is given elsewhere.[13] Finally, the normalized intensity was converted to an absolute scale (m^{-1} sterad^{-1}) using a Lupolen standard. Use of a CCD detector made it possible to work at a strain rate of 5 mm/min, collecting one frame every second. Therefore, any changes in the SAXS occurring during deformation were closely monitored.

Results

When discussing the scattering patterns, the direction parallel to the tensile axis will be referred to as the "meridian" and the perpendicular direction will be referred to as the "equator". The tensile axis was vertical in all experiments described here. Figures 2 and 3 show how the 2-D SAXS evolved during uniaxial tensile deformation of RTPMMA samples containing 10 and 20 wt % of toughening particles, respectively, and having a cross-linking density of 5% in the rubber phase. Starting with the SAXS from the undeformed sample, shown in the top left image of Figures 2 and 3, it can be seen that the pattern consists of concentric circular fringes, the most clearly visible of which are at $q \cong$ 0.0041, 0.0068, and 0.0095 Å^{-1}. These fringes are the form factor scattering of the core−shell particles, a point discussed in earlier papers on this work.[10,11] Their positions do not correspond directly to any individual repeat distance within the core−shell particles as they are a result of contributions from both the core and shell dimensions.

During deformation the fringes shifted to lower q on the meridian, and this corresponds to an increase in the real space repeat distance, d ($d = 2\pi/q$). The shift is illustrated with a particle concentration of 10 wt % in Figure 4, which shows how the meridional position of the brightest visible fringe changed during the elastic deformation of the sample. This fringe, initially at a position corresponding to a d spacing of ∼1540 Å, moved inward along the meridian, reaching a d spacing of ∼1590 Å at the specimen yield point, which occurred at approximately 1.1 mm extension. Qualitative examination revealed that the other, less distinct fringes moved in a similar manner during elastic deformation.

The tensile curves recorded simultaneously with the SAXS patterns for specimens having different particle concentrations, ranging from 10 to 40 wt %, are shown in Figure 5. At a particle concentration of 10 wt % the yield point occurred at around 1.1 mm total extension. When the particle concentration was higher, the yield point occurred at higher extension, within the range 1.4 and 2 mm. In addition to this increase in the elastic regime, Figure 5 also demonstrates that the yield stress decreased with increasing particle concentration, re-

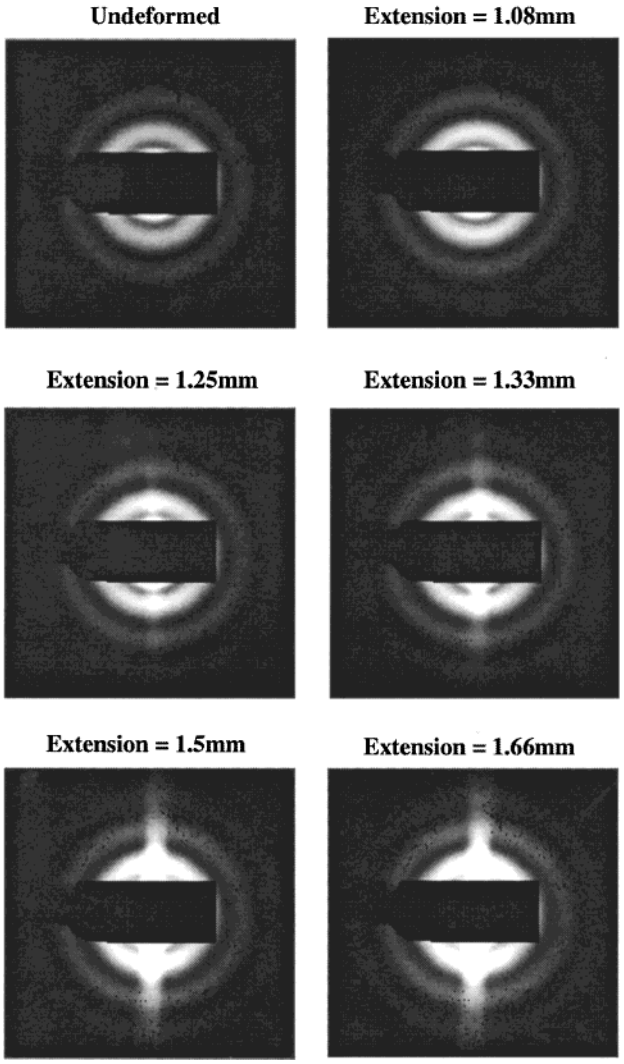

Figure 2. Scattering pattern at various stages of deformation for RTPMMA containing 10 wt % toughening particles, having 5% cross-linking density in the rubber phase. The strain rate was 5 mm/min, and the tensile axis was vertical. The q range shown here is ± 0.01 Å^{-1} in both the horizontal and vertical directions.

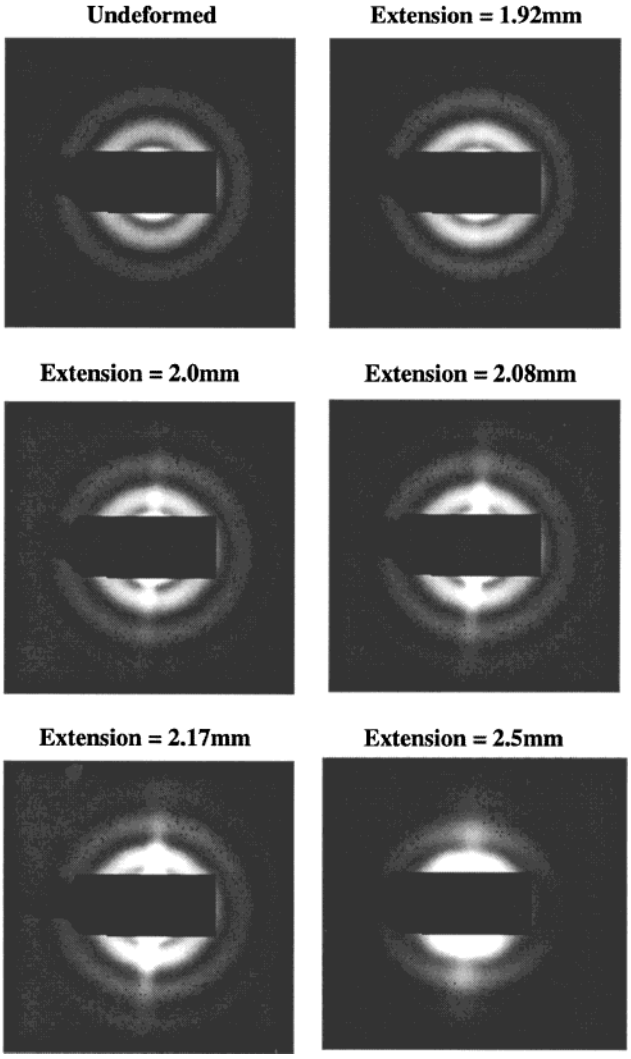

Figure 3. Scattering pattern at various stages of deformation for RTPMMA containing 20 wt % toughening particles, having 5% cross-linking density in the rubber phase. The strain rate was 5 mm/min, and the tensile axis was vertical. The q range shown here is ± 0.01 Å^{-1} in both the horizontal and vertical directions.

flecting the reduction in strength which is the penalty for the increased toughness gained by adding rubber particles.

The SAXS patterns shown in Figure 2, which are from the 10 wt % particle concentration sample, display a clear change at a sample extension of 1.25 mm with the appearance of strong, localized spots on the meridian. This distinct change happened just after the yield point which had occurred at approximately 1.1 mm extension for this sample. The development of the SAXS patterns was monitored every second throughout the tensile test, and this revealed continuous changes in the scattering pattern during yield. The spots became more intense as yield progressed, and by an extension of 1.41 mm the spots had developed into arcs, extending symmetrically either side of the meridian. In addition, meridional streaking developed with the spots, and the intensity of the meridional scattering increased. Overall, changes in the scattering were concentrated on the meridian. The only observable change on the equator was a very slight increase in intensity.

The progression of the SAXS during tensile testing of samples containing 20 wt % of particles, shown in Figure 3, was broadly similar to the 10 wt % case. During elastic deformation the fringes on the meridian moved to lower q. The meridional shift of the brightest fringe corresponds to an increase in d spacing, from its

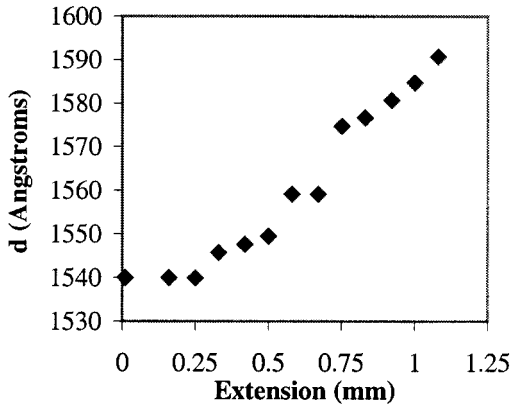

Figure 4. Meridional position of lowest q fringe, plotted in terms of real space repeat distance, d (± 5 Å), as a function of extension during elastic deformation of RTPMMA sample containing 10 wt % of particles having a 5% cross-linking density in the rubber phase.

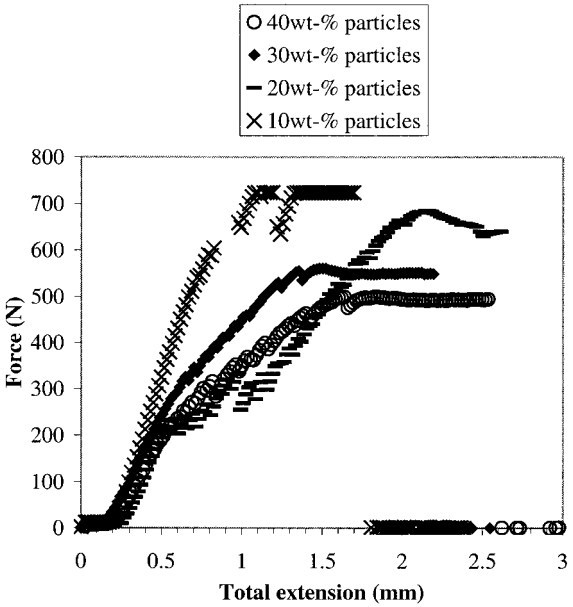

Figure 5. Effect of particle concentration on the tensile curves of RTPMMA toughened with core−shell particles which have 5% cross-linking density in the rubber phase.

initial value of ∼1510 to ∼1620 Å at the point where localized spots first appeared on the meridian. As before, the appearance of the spots occurred around the yield point, in this case at an extension of 2 mm. Also, like the 10 wt % case, the 2D SAXS for 20 wt % case changed continuously after the meridional spots first appeared. The spots gradually became arcs, extending either side of the meridian. This was accompanied by an increase in the intensity of the meridional scattering and the appearance of meridional streaking. However, when the response perpendicular to the tensile axis is considered, there is a clear distinction between the 10 and 20 wt % particle concentration samples. When the particle concentration was 20 wt %, the equatorial intensity increased at the later stages of deformation and extended to higher q, so that the overall shape of the SAXS resembled a rounded diamond, shown at an extension of 2.5 mm in the bottom right image of Figure 3.

While the sample containing 30 wt % of toughening particles behaved in a broadly similar fashion to the 20 wt % case, RTPMMA with a particle concentration of 40 wt % responded differently. Figure 6 shows the 2D scattering patterns from the 40 wt % particle concentration sample obtained at various stages of deformation. First, when comparing the undeformed particle SAXS from the 40 wt % sample with that of the 10 wt % sample, it can be seen that for the higher particle concentration the fringes are more intense, a result of the presence of more scattering centers.

Figure 7 is a plot of the meridional position of the brightest fringe, throughout the entire tensile test, for the 40 wt % particle concentration sample. This plot reveals that as the specimen was stretched the d spacing remained constant, at ∼1560 Å, during the first stages of elastic deformation, up to an extension of 1 mm. From this point, up to an extension of 1.75 mm, just before the yield point, the d spacing increased to ∼1650 Å. At the yield point, there is a clear change as the d spacing of the increases much more rapidly from ∼1710 Å just after yield to a final value of ∼2500 Å just before the sample broke. Returning to the SAXS patterns shown in Figure 6, it can be seen that with a 40 wt % particle

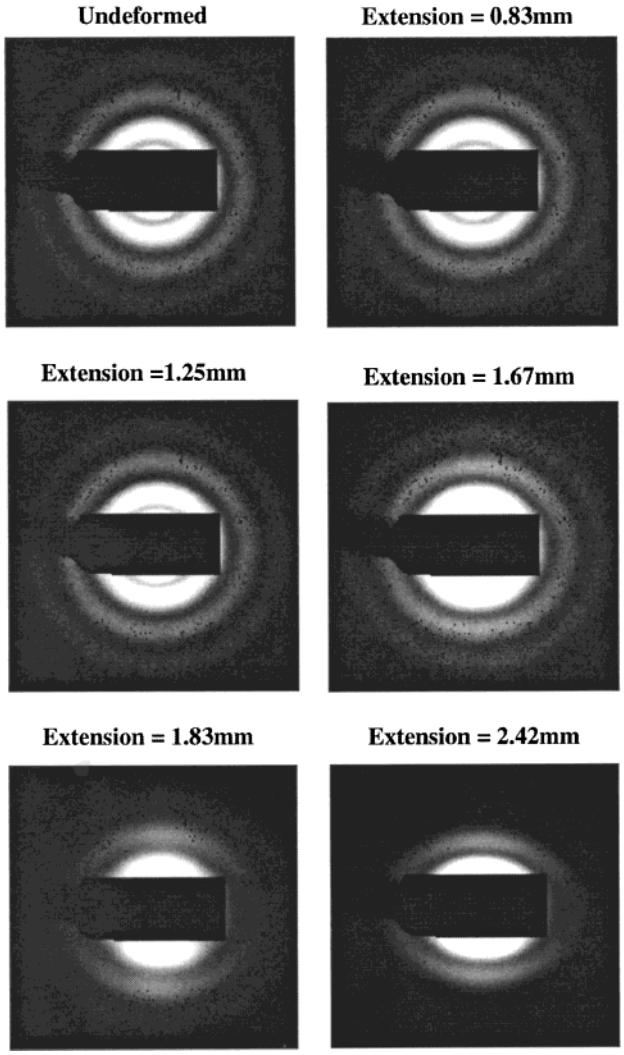

Figure 6. Scattering pattern at various stages of deformation for RTPMMA containing 40 wt % toughening particles, having 5% cross-linking density in the rubber phase. The strain rate was 5 mm/min, and the tensile axis was vertical. The q range shown here is ±0.01 Å^{-1} in both the horizontal and vertical directions.

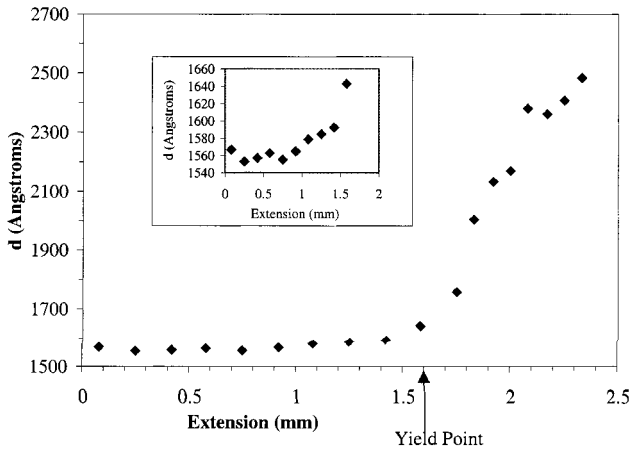

Figure 7. Meridional position of the brightest fringe, throughout the entire tensile test, for RTPMMA containing 40 wt % of particles, having 5% cross-linking density in the rubber phase (inset: detail on elastic region).

concentration localized meridional scattering does not appear until a much later stage of deformation compared with a lower particle concentration. The first signs

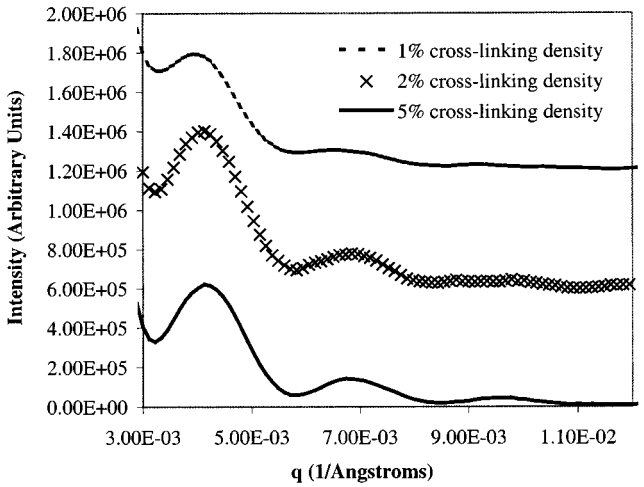

Figure 8. Form factor scattering as a meridional cut of the 2D scattering patterns for three samples having cross-linking densities of 1%, 2%, and 5%, each containing 40 wt % particles. For clarity, the curves corresponding to 1% and 2% cross-linking density have been shifted upward on the intensity scale by an arbitrary amount.

of localized meridional scattering appear beyond the yield point, at an extension of around 1.67 mm, and it does not lead to the sharp spots seen at lower particle concentration. As the plastic strain increased further, the outer scattering fringes became increasingly more blurred, as seen in the bottom two images in Figure 6. The overall shape of the scattering patterns at this late stage is approximately elliptical, with the minor axis of the ellipse parallel to the tensile axis. This shows that the particles themselves were changing shape, becoming approximately elliptical in cross section, with the major axis of the ellipse parallel to the tensile axis.

The experiments were repeated with toughening particles having lower rubber cross-linking densities of 1% and 2% over the same range of particle concentration as used before. When the cross-linking density was 2%, the samples showed very similar behavior to those having 5% cross-linking density. The exceptions to this were seen at 20 and 30 wt % particle concentration for which the localized meridional spots did not appear either at the yield point or at any stage thereafter. For these samples, the intensity became concentrated on the meridian during deformation, but not to the extent of forming spots.

When the cross-linking density was reduced further, to 1%, the fringes were less clearly defined, even prior to deformation, than for the higher cross-linking densities.

One factor, which may have contributed to these observed differences in behavior with cross-linking density, could be the effect of cross-linking on the morphology of the particles. Figure 8 shows the form factor scattering as a meridional cut of the 2D scattering patterns for three samples having cross-linking densities of 1%, 2%, and 5%, each containing 40 wt % particles. A cross-linking density of 5% produces three distinct fringes. However, on reduction of the cross-linking density to 2%, only two fringes can be distinguished. Finally, for a 1% cross-linking density, only two very weak fringes can be distinguished from the background scatter.

The observation that the fringes become less distinct with decreasing cross-linking density suggests that either the distribution of particle sizes is wider or their internal structure is less regular at lower cross-linking density. The internal interfaces of the core−shell particles may be less well-defined at lower cross-linking density as there may be more diffusion between the PMMA and rubber layer during the polymerization in the preparation of the core−shell particles. This blurring of the fringes makes interpretation of the changes in the SAXS patterns for the 1% case much more difficult.

Discussion

The 2D scattering pattern from the undeformed RTPMMA samples consisted of circular concentric fringes as seen in the top left images of Figures 2 and 3. When the toughening particle concentration was altered, the fringe positions remained constant. This is because the fringes originate from the electron density distribution within the core−shell particles. Computer simulation of the scattering from a single core−shell particle confirms that the electron density difference between the PMMA core (density 1.19 g/mm^3) and rubber shell (density 0.93 g/mm^3) is sufficient to give rise to the observed fringes.[10,11] Mathematical details of the simulation have been reported in earlier work.[11] Figure 9a compares the simulation of 2D scattering from a spherical core−shell particle having a core radius (R_c) of 800 Å and a rubber shell thickness of 450 Å (shell radius, R_s = 1250 Å), with the real scattering pattern from an undeformed RTPMMA specimen containing 10 wt % of particles. Figure 9b compares 1D meridional cuts taken from the real and simulated data shown in Figure 9a. An estimate of the range of possible particle dimensions was provided by ICI from light scattering measurements made during preparation of the toughening particles. Various combinations of core and shell dimensions within this range were tried in the simulation. It was found that a core radius of 800 Å and shell thickness of 450 Å (shell radius, R_s = 1250 Å) gave the best fit to the highest intensity peak visible in the experimental data as shown in Figure 9b. The thin PMMA outer layer was not included in the simulation as it has the same electron density as the surrounding matrix, so will not contribute to the scattering pattern.

The intensity scales of both the experimental and simulated data are arbitrary. The experimental data have been normalized, as explained in the Experimental Section, and the simulated data are for a single particle in a PMMA matrix. Furthermore, the simulation does not take into account the effects of interparticle interference, which would contribute to the very low-q part of the scattering pattern, obscured by the beamstop in these experiments. Examination of Figure 9b reveals that the fringes of the experimental scattering pattern are broadened, and overlap slightly, probably due to the range of core and shell sizes within the sample.

For all particle concentrations, the fringes moved to lower q on the meridian during elastic deformation of the RTPMMA sample. This shows that the particles themselves were stretching parallel to the tensile axis. Given that the soft rubber shell has a Young's modulus of the order of 1 MPa, it would be expected to stretch much more than the glassy PMMA core which has a Young's modulus of around 3000 MPa. This expectation was investigated by simulating uniaxial stretching of a single core−shell particle in a PMMA matrix. The particle was modeled as a pair of concentric spheres which become ellipsoidal upon stretching. The simulation is a generalization of the undeformed particle case

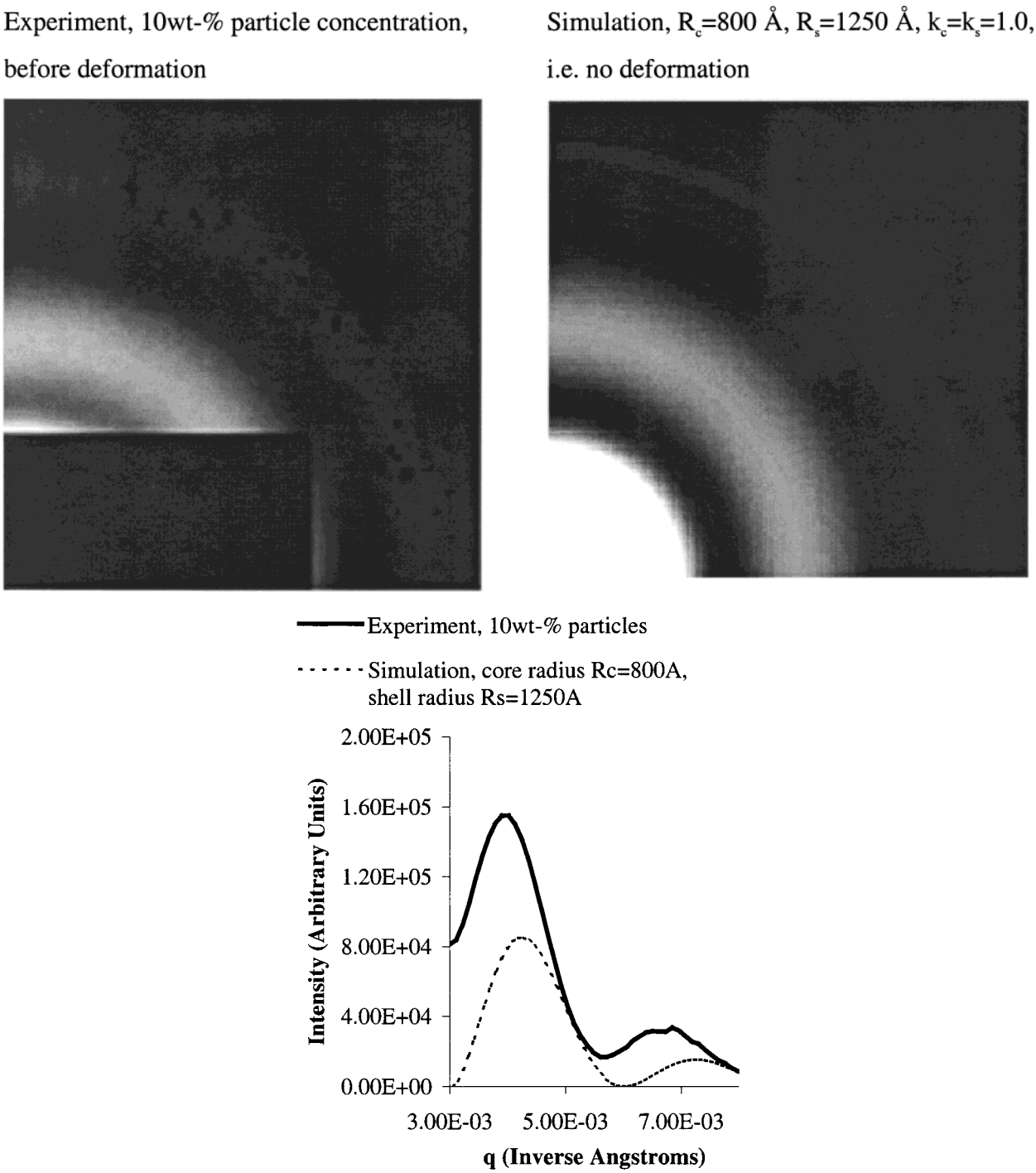

Figure 9. (a) Real SAXS pattern from undeformed RTPMMA sample and simulated pattern from a single core−shell particle (q range: 0−0.008 Å^{-1} in both directions). (b) 1D meridional cuts of the SAXS patterns shown in (a).

mentioned earlier, and mathematical details have been reported elsewhere.[11] The lengths of the major axes of the ellipses were varied, independently, to simulate different extents of core and shell deformation. For example, the simulation that most accurately predicted the meridional fringe shift seen in the 10 wt % particle concentration sample at an extension of 1.1 mm was produced by the shell deforming to an eccentricity of k_s = 1.09, while the core remained undeformed (k_c = 1.0), and this result is shown in Figure 10. Furthermore, the experimental SAXS data show that the particles deformed anisotropically, as the equatorial fringes do not shift during elastic deformation. This anisotropy was also observed for the same RTPMMA system tested at the lower strain rate of 0.5 mm/min, to be discussed in a separate paper.[13]

At and beyond the yield point, and most noticeably for the 10 wt % particle concentration specimen, there was a significant change in the scattering pattern, with the appearance of pairs of highly localized intense spots on the meridian. The position of the strongest pair of spots corresponds to the interference pattern expected from a pair of scattering centers aligned parallel to the tensile axis and spaced by approximately 1600 Å, the diameter of the PMMA core. Such a regular and well-defined spacing is consistent with the lower intensity pairs of meridional spots, occurring at higher scattering angles, being second- and third-order reflections. The

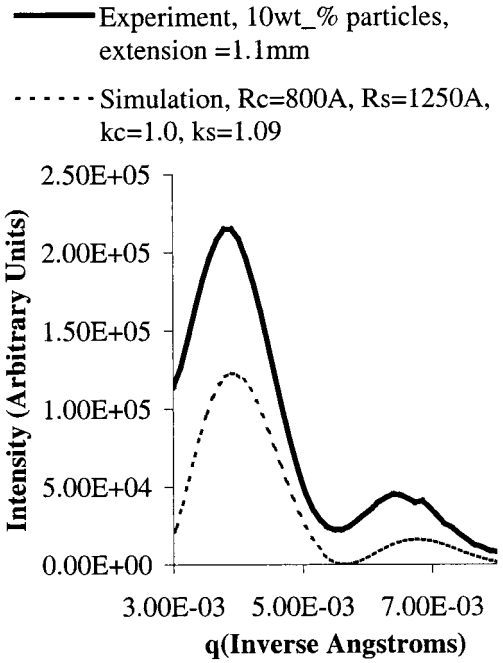

Figure 10. Comparison of meridional scattering from real RTPMMA specimen stretched to 1.1 mm total extension, with simulated scattering from a core−shell particle in which the shell is stretched while the core remains undeformed (see text for details of simulation).

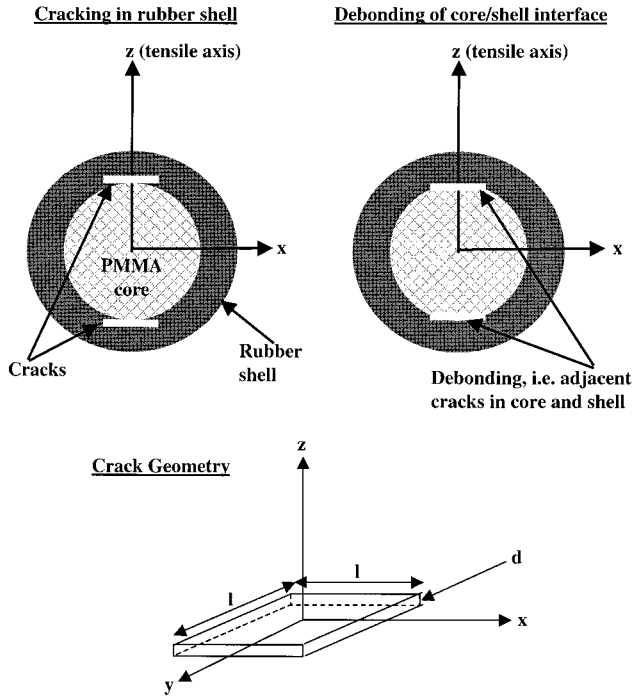

Figure 11. Geometry of the core−shell particle models used in the simulations of the scattering pattern from a particle which has undergone localized failure at, or adjacent to, the core/shell interface. Localized rubber failure was modeled as rectangular cracks as illustrated in the top left-hand diagram. The top right-hand diagram demonstrates how failure of the core/shell interface was modeled as an adjacent pair of identical rectangular cracks, one in the core and one in the shell. The lower figure shows the 3D geometry and dimensions of the cracks used in both cases.

spacing of the intense pair of meridional spots indicates the presence of scattering centers at, or immediately adjacent to, the core/shell interface. The sharpness and position of the spots show that the scattering centers were confined to the poles of the particles (the direction of the tensile axis) at this stage of deformation. These scattering centers, which emerged with the onset of yield, have two possible origins: they are either localized debonding of the core/shell interface or localized rubber failure in the shell immediately adjacent to this interface. Failure on the other side of the interface, in the PMMA core, is unlikely, as it has already been shown that the core had suffered no observable deformation by this stage. The computer simulations of the scattering pattern from a single core−shell particle in a PMMA matrix have been extended to include the two proposed forms of localized failure, interfacial debonding, or failure in the rubber adjacent to the interface. A comparison has been made between the simulated scattering patterns resulting from these two proposed modes of failure. In both cases the failure was modeled as a pair of narrow rectangular slits, centered on the meridian as shown in Figure 11. The rectangular shape of the slits is only an approximation, made for mathematical convenience. The mathematical details of these simulations of failure are given in the Appendix.

The results of simulations of localized failure, either by debonding of the core/shell interface or by rubber failure adjacent to this interface, are very similar as demonstrated in Figure 12. Therefore, it is not possible to distinguish between these two possible origins of the meridional spots from the simulated and experimental SAXS patterns alone. However, the interfacial bonding in these particles is provided by a strong copolymer graft, so rubber failure seems to be the more likely candidate.

Using this framework, accurate simulation of the SAXS pattern at yield has been achieved by modeling

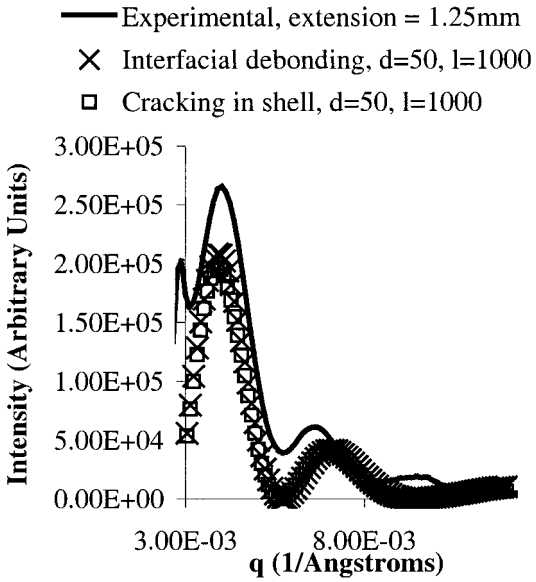

Figure 12. Results of simulations of localized failure either by debonding of the core/shell interface or rubber failure adjacent to this interface.

uniaxial stretching of the rubber shell, superimposed on localized failure in the rubber shell. The stretched shell was modeled as an ellipsoid with the major axis parallel to the tensile axis, the minor axis length set to the undeformed shell radius, and the major axis length set by an eccentricity, $k_s = 1.09$ (as shown in Figure 10). The rubber failure was simulated by a pair of rectangular slits placed at the particle poles within the shell either side of the core as shown in Figure 11. The

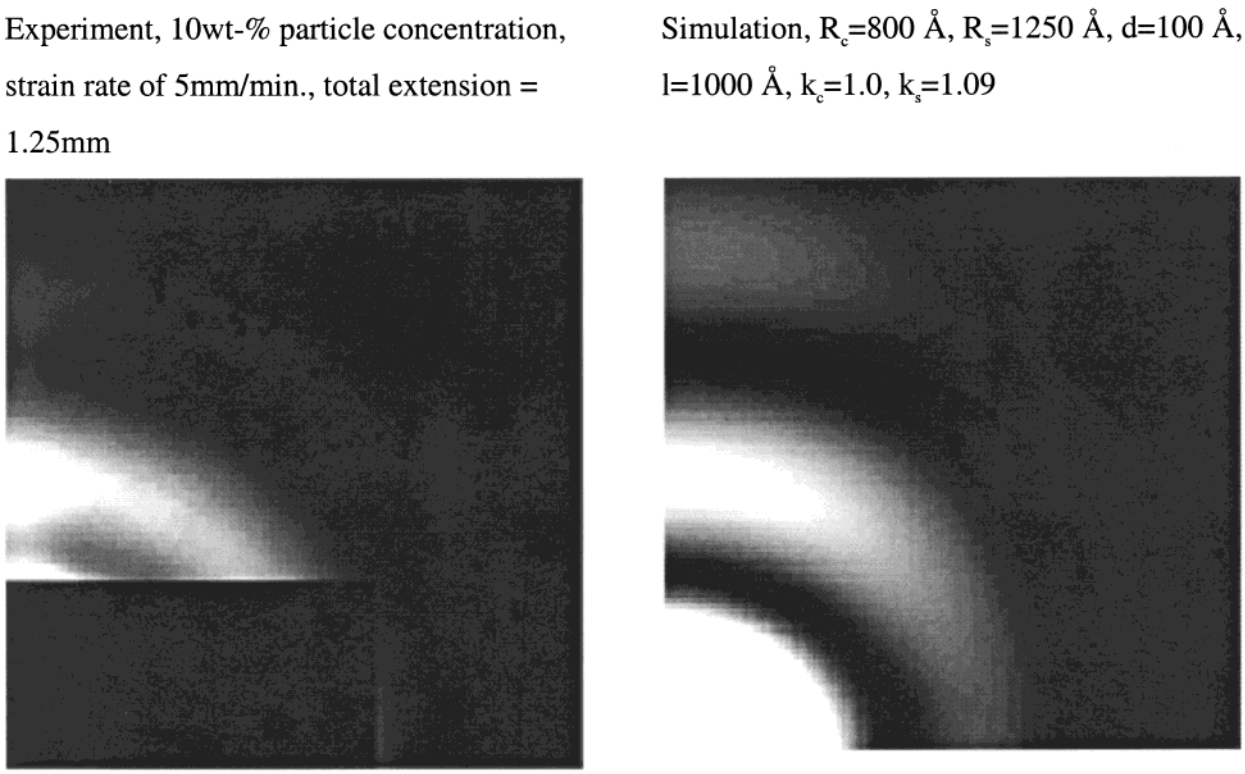

Figure 13. Comparison between the experimentally determined SAXS pattern from RTPMMA sample stretched to yield point (right-hand image) with the simulation of the SAXS pattern from a single core−shell particle in which the shell is stretched and shows localized failure (left-hand image). The tensile axis is vertical and the q range is 0−0.008 Å^{-1}, in both directions.

slit dimensions were set to $d = 100$ Å parallel to the tensile axis and to l × l with $l = 1000$ Å in the plane perpendicular to the tensile axis. The core was modeled as an undeformed sphere of radius $R_s = 1250$ Å. Figure 13 compares the 2D SAXS pattern predicted by this simulation with the real data obtained for 10 wt % particle concentration sample at 1.25 mm extension. It can be seen that there is good agreement between the predicted and experimentally determined patterns.

The SAXS results from the 10 wt % particle concentration RTPMMA sample show that the shell stretches parallel to the tensile axis, while the core remains undeformed. The localized failure can therefore be associated with stress concentration due to this difference in extensibility of the core and shell. As deformation proceeded beyond the yield point, meridional streaking appeared with the spots. This may result from spot smearing, indicating a range of core diameters. Alternatively, the streak could result from craze/bulk interface scattering occurring at the early stages of craze formation in the matrix, before fibril scattering becomes significant. However, in this instance the former explanation is thought to be more likely as no evidence for craze fibril scatter appeared at any stage of deformation, even at very high strain.

At the same time, the spots also developed into arcs, spreading either side of the meridian, indicating that the failure was growing parallel to interface between the PMMA core and rubber shell.

The positions and intensities of the fringes on the equatorial did not alter during the tensile tests, indicating that there was very little change in morphology of the particles in the direction perpendicular to the tensile axis. The SAXS patterns did not contain the cross characteristic of crazing, so crazing was not a major deformation mechanism. The deformation mechanisms proposed above are summarized schematically in Figure 14.

An increase in particle volume fraction makes the RTPMMA more compliant. Reducing the cross-linking density of the rubber layer alters the relative moduli of the rubber layer and the PMMA core. Therefore, it can be expected that changing either particle concentration or rubber cross-linking density will have an impact on the susceptibility of the particles to localized rubber failure at, or adjacent to, the core/shell interface.

When the particle concentration was increased to 20 or 30%, with 5% cross-linking density in the rubber phase, the yield point coincided with the appearance of meridional spots characteristic of localized rubber failure as seen in the 10 wt % case. Also, as before, when the sample was stretched further, the failed regions grew, both along the tensile axis and adjacent to the core/shell interface. However, at high plastic strain, the SAXS patterns developed in a different manner from that seen at the lower (10 wt %) particle concentration case. The biggest difference was seen in the equatorial scattering, which showed little change at 10 wt %, but at high particle concentration it becomes more intense on both the meridian and equator. Furthermore, the overall circular shape of the pattern changes gradually to resemble a rounded diamond. This shape could be formed by the superposition of an ellipse, resulting from the particles themselves stretching to become ellipsoidal, and a diamond which could indicate scattering from elongated cavities forming in the rubber layer. Cavitation would cause an increase in intensity because the cavities act as additional scattering centers. It has already been noted that the rubber shell deforms much more than the PMMA core. The shell stretches parallel to the tensile axis, without compressing perpendicular to the tensile axis, and the core remains undeformed.

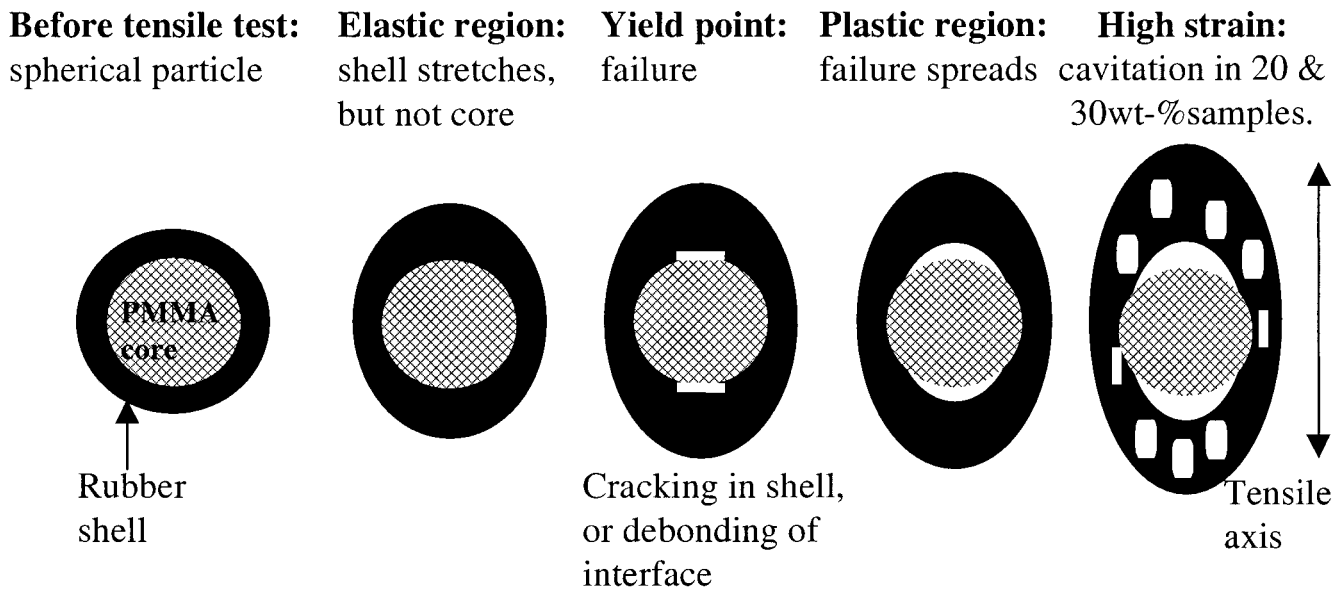

Figure 14. Schematic representation of the proposed deformation mechanisms observed at low particle concentration, 10, 20, and 30 wt %.

This suggests that the rubber shell remains bonded to the matrix and core, except at points where localized debonding occurs. Therefore, the shell experiences a hydrostatic expansion pressure, which could produce cavitation[2,3,8] within the rubber. This cavitation is consistent with no total volume change occurring in the rubber despite extensive elongation. The initial localized failure would be expected to have become quite extensive by this stage of deformation as the meridional spots can no longer be distinguished from other features. Cavitation at high strain in the 20 and 30 wt % particle concentration samples has been included in the schematic sequence of proposed deformation mechanisms shown in Figure 14. The SAXS patterns for the 10 wt % samples do not show evidence of cavitation, but this does not exclude the possibility of a very a few small cavities, insufficient to produce noticeable effects in the SAXS.

When the particle concentration was high, at 40 wt %, the deformation behavior was clearly different than that seen with lower particle concentrations. During elastic deformation of the sample, the intensity gradually became more concentrated on the meridian, but the sharp spots seen at lower particle concentration did not appear at any stage of the deformation. Beyond the yield point, the particles stretched parallel to the tensile axis to a considerably greater extent than was seen when the particle concentration was lower. This stretching was indicated by meridional shift of the lowest q fringe corresponding to an increase in d spacing from approximately 1650 Å at the yield point to a final value of ~2500 Å. Concentration of intensity on the meridian continued after the yield point, and at later stages of deformation the outer fringes became blurred. Computer simulations of scattering from this type of core−shell particle, reported earlier,[10] show that if the core and shell deform by the same amount, then the 2D SAXS shows concentric elliptical fringes. However, if the particle deformation is inhomogeneous with the rubber shell deforming more than the core, shown here to be the case, then the slight concentration of intensity on the meridian and blurring of the outer fringes are predicted.

Comparison of the SAXS from RTPMMA containing different concentrations of particles shows that when the particle concentration is low, yielding is accompanied by a breakdown of the internal structure of the particles as they show localized failure, while at higher particle concentrations the whole system becomes more compliant, allowing the particles themselves to deform substantially. It appears that transition from a stiff RTPMMA system, in which there is failure within the particles, to the more complaint system in which the particles just stretch is between 30 and 40 wt % particle concentration. At a late stage of deformation the intensity of the scattering increases, and the overall shape of the SAXS for the 20 and 30 wt % samples was a rounded diamond interpreted as indicating a change in the shape of the particles, accompanied by cavitation in the rubber phase. However, in the 40 wt % system the SAXS took on an elliptical shape, indicating that the particles change shape, becoming ellipsoidal. This reflects the increased compliance of the system at this higher particle concentration.

When the cross-linking density of the rubber phase was lowered to 1 or 2%, a different behavior was seen at all but the lowest particle concentrations. While for 10 wt % particle concentration, for both 1 and 2% cross-linking density, the meridional spots characteristic of a localized rubber failure adjacent to the interface were still seen; for higher particle concentrations they were not clearly observed. A concentration of intensity was seen to develop on the meridian during deformation, and this could be indicative of the inhomogeneous deformation of the core and shell, as discussed earlier. The evolution of the overall shape of the 2D SAXS from circular, to a rounded diamond, coupled with the increase in scattered intensity would appear to be a result of scattering from cavities forming in the rubber phase being superimposed on the form factor scattering.

Conclusions

In-situ small-angle X-ray scattering has been used to investigate deformation within core−shell rubber particles added to toughen PMMA. Different concentrations of particles and different cross-linking densities in the

rubber shell of the particles have been investigated. The scattering experiments probed a sufficiently low angle to obtain the form factor scattering of the core−shell particles. The samples were subject to uniaxial tensile deformation, at a strain rate of 5 mm/min, and use of a CCD detector allowed changes in the scattering to be closely followed during deformation.

When the cross-linking density of the rubber phase was high, at 5%, clear evidence of highly localized failure within the particles was observed. This failure could be either debonding of the core/shell interface or rubber failure in the shell immediately adjacent to the interface. This experiment cannot distinguish between these two possibilities, but given the strong bond at the interface, rubber failure is the one more likely to occur in the core−shell particles studied here. The failure was seen to begin just beyond the yield point, at which stage it was confined to the poles of the particles. As the sample was stretched further, and plastic deformation continued, the failure spread laterally, parallel to the interface. This localized failure was seen for RTPMMA specimens having particle concentrations of up to 30 wt %, with strongest evidence at lower particle concentration. For 20 and 30 wt % there was also evidence of cavities forming within the shell at the later stages of plastic deformation. When the particle concentration was increased to 40 wt %, the strong meridional spots characteristic of localized failure were not observed. At this high particle concentration the particles stretched but did not show localized failure.

On lowering the cross-linking density to 1 or 2%, the morphology of the particles was altered, as the PMMA−rubber interfaces became less well-defined. Localized rubber failure was not clearly observed, except at the lowest particle concentration. At particle concentrations above 10 wt % there was evidence for cavitation in the rubber shell being favored over localized rubber failure adjacent to the core/shell interface.

Acknowledgment. The authors thank EPSRC and ICI plc for proving financial support, Dr. Eugene Terentjev, and Mr. Samuel Kutter for assistance with the computer simulations, Professor C. B. Bucknall for helpful discussions, and Mr. P. Bone for his patience during the preparation of so many samples.

Appendix

SAXS patterns collected from low particle concentration samples during tensile deformation were characterized by the appearance of a pair of meridional spots coincident with the yield point of the tensile curve. The spots were spaced by ∼1600 Å, which is the core diameter, and higher-order reflections were also visible. Therefore, it is postulated that highly localized scattering centers at, or immediately adjacent to, the core/shell interface are created at the poles of the particle at the yield point. This idea has been tested by simulating the failure as a pair of cracks at the poles of the particle, positioned either side of the core at the interface, or in the softer rubber shell immediately adjacent to the interface. Both interfacial failure and failure within the shell were compared. The geometries of the cracked particle used in both cases for the simulation are shown in Figure 11.

Case 1: A Pair of Polar Cracks, Adjacent to the Core/Shell Interface, in the Shell. Crack dimensions are l × l in the *xy* plane and *d* in the *z* direction, which is parallel to the tensile axis. The condition that $l \gg d$ applies. ρ is the density of the medium in which the crack appears, in this case the rubber shell. This assumes that the crack is empty, but a crack containing "thinned rubber", for example, could in principle be modeled by taking some fraction of ρ. The structure factor of a single crack is given by

$$F_c(q_x,q_y,q_z) = \rho\int\int_{vol}\int e^{i(q_x x,q_y y,q_z z)}\,dx\,dy\,dz = \rho\int_{-l/2}^{l/2} e^{i(q_x x)}\,dx \int_{-l/2}^{l/2} e^{i(q_y y)}\,dy \int_{-d/2}^{d/2} e^{i(q_z z)}\,dz$$

$$= \rho l^2 d\,\frac{\sin(q_x{}^l/_2)}{q_x{}^l/_2}\,\frac{\sin(q_y{}^l/_2)}{q_y{}^l/_2}\,\frac{\sin(q_z{}^d/_2)}{q_z{}^d/_2}$$

Defining the image plane as q_x, q_z, with $q_y = 0$, gives

$$F_c(q_x,q_z) = \frac{4\rho l}{q_x q_z}\sin(q_x{}^l/_2)\sin(q_z{}^d/_2)$$

For a pair of slits, separated by 2*a*, F_c can be convoluted with a pair of delta functions to give the structure factor, G_c, of the pair of slits:

$$G_c(q_x,q_z) = 2\cos(q_z a)\,F_c(q_x,q_z) = \frac{8\rho l}{q_x q_z}\sin(q_x{}^l/_2) \times \sin(q_z{}^d/_2)\cos(q_z a)$$

To model rubber failure adjacent to the core/shell interface, the slit separation is given by $2a = 2(R_c + d/2)$.

The structure factor of the cracked particle $F_{cracked}$ is then modeled using the structure factor for the core−shell particle, F_{csp}, and G_c:

$$F_{cracked} = F_{csp} - G_c$$

Details of the calculation of F_{csp} are given in another paper,[11] and the result is

$$F_{csp}(q_x,q_z) = (2\pi)^{3/2}(\rho_c - \rho_s)\left(\frac{R_c{}^{3/2}k_c}{(q_x{}^2 + (k_c q_z)^2)^{3/4}}J_{3/2} \times [R_c\sqrt{q_x{}^2 + (k_c q_z)^2}] - \frac{R_s{}^{3/2}k_s}{(q_x{}^2 + (k_s q_z)^2)^{3/4}}J_{3/2} \times [R_s\sqrt{q_x{}^2 + (k_s q_z)^2}]\right)$$

where k_c and k_s are respectively the core and shell eccentricities, and $J_{3/2}$ is a Bessel function of the order $^3/_2$.

The simulated SAXS pattern of a cracked core−shell particle was obtained by calculating the scattering intensity, $I\alpha|F_{cracked}|^2$.

Case 2: Localized Debonding of the Core/Shell Interface, at the Poles of the Particles. The debonded regions were modeled as cracks in a manner very similar to that described in the previous case. Each debonded region was treated as a pair of adjacent cracks, one in the core and one in the shell. Both cracks were *d*/2 wide in the *z* (tensile axis) direction and had dimensions l × l in the *xy* plane. The structure factor ($G_{debonded}$) of a pair of debonded regions, one at each pole of the core, was then modeled by convoluting the structure factor of 1 debonded region with a pair of delta

functions.

$$G_{\text{debonded}}(q_x,q_z) = \frac{8(\rho_c + \rho_s)l}{q_x q_z} \sin(q_x{}^{l}/_{2}) \times \sin(q_z{}^{d}/_{4})(\cos(q_z a) + \cos(q_z b))$$

where $a = R_c - d/4$ and $b = R_c + d/4$, and ρ_c and ρ_s are the densities of the core and shell, respectively.

References and Notes

(1) Bubeck, R. A.; Buckley, D. J.; Kramer, E. J. *J. Mater. Sci.* **1991**, *26*, 6249−6259.
(2) Lazzeri, A.; Bucknall, C. B. *J. Mater. Sci.* **1993**, *28*, 6799−6808.
(3) Bucknall, C. B.; Karpodinis, A.; Zhang, X. C. *J. Mater. Sci.* **1994**, *29*, 3377.
(4) Magalhaes, A. A. M.; Borggreve, J. R. M. *Macromolecules* **1995**, *28*, 5841−5851.
(5) Parades, E.; Fischer, E. W. *Makromol. Chem.* **1979**, *180*, 2707−2722.
(6) Brown, H. R.; Kramer, E. J. J. *Macromol. Sci., Phys.* **1981**, *19B*, 487.
(7) Okamoto, Y.; Miyagi, H.; Mitsui, S. *Macromolecules* **1993**, *26*, 6547.
(8) Lazzeri, A.; Bucknall, C. B. *Polymer* **1995**, *36*, 2895−2902.
(9) Shirrer, R.; Fond, C.; Lobbrecht, A. *J. Mater. Sci.* **1996**, *32*, 6409.
(10) He, C.; Donald, A. M.; Butler, M. F.; Diat, O. *Macromol. Sci. Symp.* **1996**, *112*, 115−122.
(11) He, C.; Donald, A. M.; Butler, M. F.; Diat, O. *Polymer* **1998**, *39*, 659−667.
(12) He, C.; Donald, A. M.; Butler, M. *Macromolecules* **1998**, *31*, 158−164.
(13) Sferrazza, M.; Crawshaw, J.; Donald, A. M., manuscript in preparation.

MA002060V